Published in final edited form as:

Nat Immunol. 2019 May ; 20(5): 602–612. doi:10.1038/s41590-019-0342-0.

Lymph Node Conduits Transport Virions for Rapid T Cell Activation

Glennys V. Reynoso[1], **Andrea S. Weisberg**[2], **John P. Shannon**[1], **Daniel T. McManus**[1], **Lucas Shores**[3], **Jeffrey L. Americo**[2], **Radu V. Stan**[4,5], **Jonathan W. Yewdell**[3,*], and **Heather D. Hickman**[1,*]

[1]Viral Immunity and Pathogenesis Unit, Laboratory of Clinical Immunology and Microbiology (LCIM), National Institutes of Allergy and Infectious Diseases (NIAID), National Institutes of Health (NIH), Bethesda, MD 20892.

[2]Genetic Engineering Section, Laboratory of Viral Diseases (LVD), NIAID, NIH, Bethesda, MD 20892.

[3]Cell Biology Section, LVD, NIAID, NIH, Bethesda, MD 20892.

[4]Department of Biochemistry and Cell Biology, Geisel School of Medicine at Dartmouth, Lebanon, NH 03756.

[5]Department of Pathology, Geisel School of Medicine at Dartmouth, Lebanon, NH 03756.

Abstract

Despite intense interest in antiviral T cell priming, the routes of virion movement in lymph nodes (LNs) are imperfectly understood. Current models fail to explain how virus-infected cells rapidly appear within the LN interior after viral infection. To better understand virion trafficking in the LN, we determined virion and infected-cell locations after vaccinia and Zika virus administration. Notably, many rapidly infected cells in the LN interior were adjacent to LN conduits. Using confocal and electron microscopy, we clearly visualized virions within conduits. Functionally, $CD8^+$ T cells rapidly and preferentially associated with vaccinia virus-infected cells deeper in the LN, leading to T cell activation in the LN interior. These results reveal that it is possible for even large virions to flow through LN conduits and infect dendritic cells within the T cell zone to prime $CD8^+$ T cells.

One sentence summary:

Virions can access lymph node conduits.

*Correspondence to: Jonathan W. Yewdell (jwyewdell@nih.gov) or Heather D. Hickman (hhickman@nih.gov).

AUTHOR CONTRIBUTIONS

H.D.H. conceived the project. H.D.H., R.V.S., and J.W.Y. secured funding. H.D.H., G.V.R., A.S.W., J.P.S., D.T.M., L.S., J.L.A. performed experiments and analyzed data. R.V.S. provided mice and technical expertise. H.D.H. wrote the manuscript. H.D.H., R.V.S., and J.W.Y. edited the manuscript.

COMPETING INTERESTS

The authors declare declare no competing interests as defined by Nature Research, or other interests that might be perceived to influence the results and/or discussion reported in this paper.

Lymph nodes (LNs), the site of initiation of adaptive immune responses, are highly organized structures optimized for receiving and presenting foreign antigens to naïve T and B lymphocytes. The movement of antigen to and within the LN dictates the activation of lymphocytes in ways that are incompletely understood and are poised to impact the magnitude and effectiveness of the immune response. Despite the importance of LN antigen presentation, antigen movement in the LN has primarily been studied at spatial resolution after challenge with non-infectious antigens [1, 2, 3, 4, 5, 6, 7, 8]. Though the list is increasing, only a handful of viruses have been directly visualized in the infected LN, including vaccinia virus (VACV) and modified vaccinia Ankara (MVA) (for examples of studies imaging these viruses, see [9, 10, 11, 12, 13, 14, 15]).

Virions traffic to the LN within minutes after deposition into peripheral tissues [10]. Virions present in the interstitial fluid flow into a network of unidirectional, afferent lymphatic vessels and are transported to the LNs. Conveyed virions are deposited into the LN subcapsular sinus (SCS), a large cavity underneath the LN capsule lined with lymphatic endothelial cells (LECs) and phagocytic SCS macrophages [10, 16, 17, 18]. These macrophages represent the first line of defense against invading pathogens and, in their absence, both viruses and bacteria can escape the LN and infect peripheral tissues[11, 17]. Though less numerous than macrophages, sinus-associated dendritic cells (DCs) also access particulate antigens in LN sinuses [5, 19, 20]. Particulates not acquired by phagocytic cells continue through nodal sinuses before exiting through the efferent lymphatics [20].

Antigen-presenting cells (APCs) within the LN acquire viral antigen via one of several routes defined largely through studies utilizing protein or polysaccharide administration. Although lymph-borne proteins are deposited into the SCS, the SCS floor is lined by LECs that prevent free access to the LN paracortex. Low-molecular weight proteins (> 70 kDa) can access the LN reticular conduit system that connects the SCS to the paracortex [1, 21]. The conduits consist of a core of organized collagen fibrils ensheathed by fibroblastic reticular cells (FRCs), forming a channel through which small proteins are transported. The conduit system runs throughout the LN, but is less dense in the B cell follicles and deep T cell zone [22, 23].

The conduits are not contiguous, with approximately 10% of the conduit surface having gaps in FRCs covered by DCs [3]. Conduit-associated DCs access luminal contents and can present conduit-transported antigens to naïve T cells. Although the biophysical properties of the core of collagen fibrils were originally thought to control the size limitation for conduit entry, it was recently shown that the LEC protein plasmalemma vesicle-associated protein (PLVAP) establishes the 70 kDa “filter” [6]. PLVAP proteins on LECs form structures at the conduit-entry sites in the SCS thought to prevent anything over 70 kDa from accessing the conduits. In accordance, a recent study showed that subcutaneously injected immunoglobulin M (IgM, ~150 kDa) was excluded from the conduits; in contrast, IgM injected directly into the LN paracortex could enter the conduit system [8].

Owing to their large size, virions are not believed to gain entry to LN paracortex via conduit transport. After subcutaneous injection, VACV virions arrive at the LN within minutes, are deposited into the SCS, and infect a sessile layer of macrophages in the SCS floor [10, 13].

Virions not captured by SCS-resident cells continue through LN sinuses, but should be unable to access the LN paracortex. We analyzed virion transport in the LN after infection with VACV and Zika virus (ZIKV). VACV is a large DNA virus that is used both to study antiviral immunity in the draining LN and as a human vaccine vector [24, 25]. Zika virus is a small RNA virus responsible for recent explosive human outbreaks [26]. Here, we show that multiple viruses (even VACV, the largest human viral pathogen) can enter LN conduits and infect paracortical DCs, leading to rapid and direct T cell priming in the LN paracortex.

Results

Virally infected cells are located proximal to conduits

Wild-type vaccinia virus (VACV) and its related, non-replicating strain modified vaccinia Ankara (MVA) have been employed extensively to visualize antiviral immunity in the LN. Additionally, both VACV and MVA are currently inoculated into humans, the latter serving as a vector for recombinant proteins [25]. Many imaging studies and vaccine trials administer 10^8 pfu or greater of VACV or MVA (for examples see [27, 28]), while immunologic studies often infect at lower viral doses. It is currently unclear how the dose of virus affects the spatial organization of T cell priming in the LN as such spatial analyses have not been systematically compared. Therefore, we carefully quantified the location of VACV- and MVA-infected cells in the draining LN across viral doses (Fig. 1). As previously reported, using viral promoter-driven fluorescent protein expression (influenza virus nucleoprotein-SIINFEKL-enhanced green fluorescent protein (NP-S-eGFP), a fusion protein with nuclearly localized GFP along with the SIINFEKL determinant from ovalbumin), we detected robust viral infection of cells in the peripheral subcapsular sinus (SCS) and interfollicular area (IFA) cells within 8 h of infection with either virus [10] (Fig. 1a,b). Staining for VACV antigen confirmed that GFP expression was produced in conjunction with VACV proteins (Supplementary Fig. 1) rather than being acquired by uninfected cells. Unexpectedly, at higher viral doses, we visualized numerous virus-infected cells deeper within the LN paracortex (Fig. 1a,b and Supplementary Fig. 2).

We next quantified the location of infected cells in the SCS and IFA region (SCS&IFA), B cell follicles, T cell zone, or the medulla of frozen sections of LNs 8 h after footpad infection with 10^8 pfu of VACV or MVA (Fig. 1c,d). We classified different LN anatomical regions by staining sections with antibodies against the LN stroma (ERTR7 recognizing reticular fibroblast antigen, red), the lymphoid sinuses (Lyve-1 recognizing LECs, white), and B cells (B220, blue) as previously described [18]. Although most infected cells were located in the SCS and IFA region followed by the medullary sinuses, on average ~11% of VACV-infected cells and ~4% of MVA-infected cells were present in the T cell zone (Fig. 1d). Higher magnification images showed VACV-infected cells contacting LECs in the SCS and IFA region and in sinuses (Fig. 1e, right), but also nodal conduits in the T cell zone located distally from apparent LECs (Fig. 1e, left). Quantitation of cells touching either conduits or sinuses revealed that approximately 20% of infected cells contacted only conduits; these numbers include cells located in the SCS and IFA region as well as in the T cell zone (Fig. 1f). Collectively, these data demonstrate that infected cells are present in the

LN T cell zone after infection with 10^8 pfu of VACV and that paracortical infected cells closely associate with conduits.

Paracortical-infected cells appear rapidly

To understand how virus-infected cells arrived in the LN paracortex, we next kinetically analyzed LNs after infection with 10^8 pfu of VACV (Fig. 2). Using a GFP antibody, we detected VACV-infected cells in the SCS and IFA region, T cell zone, and medulla by 1 h post infection (Fig. 2a). We continued to observe VACV-infected cells in the T cell zone throughout the next 7 h of infection (Fig. 2b and Supplementary Fig. 3), suggesting that these cells were infected soon after viral inoculation and then remained associated with conduits. Based upon these data and those from other laboratories [10, 13], we summarize the following timeline of nodal VACV infection after subcutaneous injection: VACV virions arrive in the draining LN within minutes (possibly seconds). Infected cells can be detected in the LN after staining for GFP within an h after footpad administration of 10^8 pfu of virus. After 4 h, VACV-infected cells can be detected simply by the robust expression of GFP. Within 12–24 h, VACV-infected SCS macrophages pyroptose as a result of inflammasome activation [13, 14]. Together, these data demonstrate that VACV-infected cells can be detected in the LN paracortex rapidly after infection, and detection is enhanced by the accumulation of virally expressed GFP.

Vaccinia virions are transported by nodal conduits

The infection of T cell-zone cells so soon post infection led us to question whether virions could be transported in the LN conduits running from peripheral sinuses. To investigate this hypothesis, we first conjugated purified VACV to Alexa 647 dye and extensively purified virions to remove residual dye. Using confocal microscopy, we visualized labeled virions (white) in LN conduits within 3–5 min of injection (Fig. 3a,b). We next conjugated purified VACV to 10 nm gold particles, injected 10^8 pfu in the footpad, and analyzed LN sections by electron microscopy (EM) 3–5 min after injection. Electron micrographs showed numerous instances of gold particle-labeled VACV virions within conduits (Fig. 3c and Supplementary Fig. 4). Thus, VACV virions can be accommodated by LN conduits.

In the LN, the protein PLVAP is expressed on LECs in the SCS that line the entrance of conduits[6] as well as on other stromal cell populations. On LECs, this protein forms structures at the entrance of conduits that act as a molecular sieve, blocking conduit entry of large proteins. To determine if PLVAP also regulated VACV entry into LN conduits, we injected Alexa-647 labeled VACV into the footpad of mice in which *PLVAP* was conditionally deleted from LECs but remained intact on other cell types (*Plvap*$^{fx/fx}$ *Prox1*-CreERT$^{tg/+}$ [29]) (Fig. 3d). Conditional deletion of *Plvap* from LECs greatly increased the number of conduit-associated virions. Likewise, *Plvap* conditional deletion enhanced the number of T cell-zone infected cells 8 h post infection (Fig. 3e). Together, these data indicate that VACV virions can be accommodated by nodal conduits if the virions can enter, and that many virions are normally excluded from conduit entry by PLVAP present on LECs.

VACV infects conduit-associated paracortical DCs

Immature dendritic cells (DCs) are located in close proximity to LN conduits and can acquire small proteins from the conduit lumen for presentation to T cells [3]. Because immature DCs are susceptible to VACV infection *ex vivo*, we next sought to determine whether conduit-associated DCs could acquire VACV virions. Thus, we performed multiplex staining and confocal microscopy on LN sections harvested 8 h after footpad infection with 10^8 pfu of VACV, allowing the identification of conventional DC1s (cDC1s: CD8α$^+$, CD205$^+$, XCR1$^+$) and conventional DC2s (cDC2s: CD11b$^+$, CD172$^+$) (Fig. 4). As previously described, a majority of VACV-infected cells were sinus-resident macrophages [9, 10] (Fig. 4e), however infected cDC1s and cDC2s could also be found associated with lymphatic sinuses (Fig. 4b,c). In the paracortex, we identified infected cDC1s associated with conduits (Fig. 4d). Staining with individual markers (Supplementary Fig. 5) corroborated findings with multiplex staining. These data show that conduit-associated cDC1s in the T cell zone are infected by VACV.

Conduits transport ZIKV virions

To determine if other viruses could also enter LN conduits, we next performed similar imaging experiments after infection with ZIKV, a small RNA virus with a virion diameter of approximately 50 nm [30]. We infected *Ifnar*$^{-/-}$ mice (a standard model of ZIKV infection) with 10^4 pfu of ZIKV H/PF/2013 in the footpad and harvested the popliteal LN 24 h post infection (Fig. 5). Confocal imaging revealed ZIKV-infected cells in the LN paracortex (Fig. 5a), although it should be noted that at this time post infection, infected cells could result from infection within the LN or migration from the tissue. Multicolor staining for DC subsets (Fig. 5b) revealed both ZIKV-infected cDC1 (Fig. 5d) and cDC2 (Fig. 5c). Because cDC1 are non-migratory, conduit-associated cells, this observation suggested that conduits could transport ZIKV virions.

We next performed EM analysis ZIKV-infected LNs, imaging numerous instances of ZIKV in LN conduits (Fig. 5e and Supplementary Fig. 6). Thus, like VACV, ZIKV can enter the nodal conduits and conduit-associated ZIKV-infected DCs can be identified in the LN paracortex. These data demonstrate that conduit transport is not a unique feature of VACV and can occur at much lower viral doses.

T cells are rapidly activated by paracortical VACV-infected cells

VACV-specific CD8$^+$ T cells are rapidly activated via direct priming in the peripheral interfollicular areas of the LN under low-virus dose [10]. To determine how T cell priming proceeds when virus-infected cells are present both at the LN periphery and the paracortex, we examined the location of T cell clusters around infected cells, an oft-used indicator of cognate antigen presentation in imaging studies. Prior to infection, we transferred 10^6 OT-I CD8$^+$ T cells (T cell-receptor-transgenic cells that are H-2 K^b-SIINFEKL-specific[31]) and infected with VACV either expressing or lacking SIINFEKL (Fig. 6). OT-I CD8$^+$ T cells could be observed clustering around conduit-associated, VACV-infected cells (an example near a high endothelial venule (HEV) is shown in Fig. 6a).

As naïve T cells enter through paracortical HEVs, we next queried whether the location of infected cells in this nodal region yielded a temporal advantage for $CD8^+$ T cell activation. Again, we transferred 10^6 dsRed OT-I $CD8^+$ T cells and analyzed dissociated LNs by flow cytometry 8 h post infection (Fig. 6b). Approximately 70% of transferred cells upregulated the activation marker CD69 at the highest dose of virus, while only ~20% of T cells were activated with even a 10-fold decrease in virus. By 24 h post-infection, however, all doses of virus equally activated OT-I $CD8^+$ T cells until the inoculum decreased to 10^5 pfu, at which dose there was a slight decrease in CD69 expression (Fig. 6c). Thus, sufficient antigen was present in the node at 10^6 pfu to activate all transferred T cells, yet T cells were activated the most rapidly at the dose of virus yielding the most paracortical virus-infected cells. After infection with 10^8 pfu of VACV or MVA, a majority of virus-infected cells in the paracortex were contacted by OT-I $CD8^+$ T cells, in contrast to a far lower percentage of SCS-and-IFA-region-infected cells (Fig. 6d). This observation suggests that paracortical infected cells are preferentially contacted by T cells, either because of a functional advantage or simply due to ease in access.

We next quantified CD69 mean fluorescent intensities (MFI) on OT-I $CD8^+$ T cells in sections of LNs harvested 8 h after infection with 10^8 pfu of VACV (Fig. 6e-h and Supplementary Fig. 7). OT-I $CD8^+$ T cells in clusters around infected cells expressed abundant CD69 that was detectable by microscopy (Fig. 6g). We quantified the percentage of activated T cells (with an MFI ≥ 50) in each region of the LN at 10^8 pfu in 10 LN sections (Fig. 6e). Approximately 40% of all nodal T cells were activated in the T cell zone, while less than 20% were activated in the SCS and IFA region. Accordingly, ~54% of the activated T cells were in paracortex (Fig. 6f). In contrast, infection with lower viral doses resulted in activated cells primarily in the SCS and IFA region (Supplementary Fig. 8). Next, we analyzed the CD69 MFI only on activated OT-I $CD8^+$ T cells (with an MFI ≥ 50) across a single node (Fig. 6h and Supplementary Figure 7). The MFI of activated T cells in the paracortex was significantly higher than those at the periphery (average of 105 *vs.* 89, respectively). Similar to transgenic T cells, activated polyclonal $CD8^+$ T cells also predominated in the T cell zone (Fig. 6i,j). Collectively, these data show that T cell zone VACV-infected cells more rapidly activate $CD8^+$ T cells than those in other nodal regions.

Lower VACV doses activate T cells in the LN paracortex

To determine if conduit transport also results in T cell activation after infection with lower VACV doses, we imaged LNs harvested 8 h after infection with 10^6 pfu VACV (Fig. 7). As expected, most infected cells were located in the SCS and IFA region (see also Supplementary Fig. 8), however, we detected one or more paracortical, conduit-associated VACV-infected cell in most LN sections (Fig. 7a). We next transferred 10^6 dsRed OT-I $CD8^+$ T cells, infected with 10^6 pfu of VACV, and harvested LNs 8 h later (Fig. 7b). While a majority of activated OT-I $CD8^+$ T cells were present in the SCS and IFA region, we also detected T cell clustering and upregulation of CD69 around paracortical infected cells. Confocal analyses of DC subsets (as in Fig. 4) revealed that cDC1 in the paracortex could also be infected at lower VACV doses (Fig. 7c). These data show that conduit transport of VACV for T cell activation also occurs at lower viral doses, albeit with greatly reduced frequency.

T cells have a temporal trafficking advantage

We next transferred OT-I CD8$^+$ cells and infected footpad with different doses of VACV-expressing SIINFEKL (Fig. 8). 24 h after footpad infection, we infected in the ear pinna with VACV lacking SIINFEKL (we have previously shown that this infection schedule results in antigen-independent recruitment of activated T cells into the skin but eliminates the possibility of T cell activation in the ear-draining LN [32]). Four days after footpad infection, we removed ears and analyzed the number of recruited T cells by flow cytometry (Fig. 8a). After infection with 10^8 pfu of VACV, we detected significantly higher numbers of OT-I CD8$^+$ T cells in the skin, suggesting that footpad infection with the highest dose of virus leads to a temporal advantage in trafficking to infected peripheral tissue. Likewise, after footpad infection followed by skin infection with VACV expressing SIINFEKL, we detected higher numbers of IFN-γ-producing T cells in the skin directly *ex vivo* (e.g. without restimulation) at the highest virus dose (Fig. 8b). Thus, infection with the highest viral dose results in a temporal advantage for peripheral effector cell recruitment, consistent with early activation in LN paracortex.

Discussion

Our data provide evidence that virions can enter and move through LN conduits, infecting paracortical DCs which rapidly activate antiviral CD8$^+$ T cells. Former studies examining conduit transport of antigen reproducibly demonstrated that the bulk of large molecular weight proteins and dextrans are excluded from conduit entry, suggesting a limited role for conduits in the delivery of large, complex antigens such as viruses to the LN paracortex [1, 3, 6, 7, 8]. Collectively, these studies utilized fluorescently labeled proteins or dextrans that could be detected by confocal microscopy as they filled the conduits. In these systems, very small numbers of proteins or dextrans entering the conduits would not be easily detectable by fluorescence and would not likely yield enough antigen to activate paracortical T cells. In contrast, cellular infection with a single VACV virion rapidly generates sufficient levels of viral peptide:MHC complexes for T cell activation and the translation of many copies of viral proteins allows the detection of single infection events within 4 h of infection. Thus, viruses serve as the perfect tool to uncover a previously unappreciated aspect of conduit function.

Paracortical cDC1s have high capacity for priming antiviral CD8$^+$ T cells in *ex vivo* studies [33, 34], yet these cells are primarily positioned in the deep paracortex [5, 35]. Without nodal viral replication, it is unclear how these paracortical cDC1s can rapidly respond to infection because most should not access virus in sinuses. For protein antigens, the location of MHC-I specialized DCs in areas with limited antigen delivery substantially hinders the CD8$^+$ T cell response compared to that of CD4$^+$ T cells [7]. Virion transport by conduits has the potential to overcome these problems by delivering infectious virions to paracortical DCs.

The role of the FRCs in the LN extends beyond forming the conduits. Indeed, FRC function is critical for normal immunologic health during both homeostasis and infection. In uninfected LNs, FRCs produce cytokines and chemokines that attract and maintain DCs, naïve T cells, and B cells [36, 37, 38]. FRCs provide a scaffold necessary for cellular motility and establish LN anatomical subregions including the B cell follicles [39]. FRCs also control

rapid LN expansion during infection and inflammation, proliferating and stretching to accommodate LN hypertrophy [40, 41, 42]. Because of the myriad FRC functions, any perturbation of the conduit network can dramatically impact the immune response.

Some viruses target the LN FRC network either directly or indirectly. LNs undergo a marked fibrosis during HIV and SIV infection in which collagen replaces the FRC network which can no longer provide IL-7 to T cells, leading to T cell depletion[42, 43]. The FRCs are directly infected by the murine pathogen LCMV, resulting in upregulation of PD-L1, slowing viral clearance and increasing immunopathology [44]. Effector $CD8^+$ T cells also eliminate LCMV-infected FRCs, limiting the immune response to new antigens [45, 46]. A number of other viruses also directly infect the FRC network, including Ebola, Marburg, and Lassa, and infected FRCs may propagate infectious virus leading to complete destruction of lymphoid tissues [47, 48, 49, 50]. Our data suggest that infection by FRC-tropic viruses may be hastened after conduit transport of virions deeper into the paracortex through increased pathogen accessibility to downstream, uninfected FRCs. However, in contrast to the aforementioned viruses, VACV and ZIKV do not robustly infect FRCs. The rapid appearance of VACV virions in the conduits (within 3 minutes post-footpad injection) indicates that virions can access the conduits in the absence of FRC infection.

Although FRCs are not directly infected by VACV, infection results in LN hypertrophy and remodeling of the FRC conduits. In seminal studies, Gretz *et al.* demonstrated that VACV-induced LN hypertrophy did not disrupt the size-exclusion of the conduit system [1]. To demonstrate maintenance of size-exclusion during infection, small (10 kDa) and large (70 kDa) fluorescent dextrans were co-injected 8 h after infection with 10^7 pfu of VACV. Even though LNs had swelled to ~40% larger than their original size, the pattern of tracer distribution remained unchanged. Thus, virus-induced conduit remodeling is unlikely to account for the presence of virions in the conduits within 8 h post infection, and even less likely for our EM studies, which were performed 3–5 minutes post infection. Because we observed both VACV and ZIKV within conduits, it seems improbable that a specific/single viral surface protein mediates access to the conduits. Future studies will determine the extent to which conduit entry is an active process exploited by viruses *vs* simply a general feature of conduit biology.

How do virions gain entry to the conduits? The endothelial protein PLVAP was recently shown to form a structure acting as a “sieve,” allowing only small molecular weight proteins to enter the conduits [6]. Importantly, conditional deletion of PLVAP afforded conduit entry to proteins 10-fold larger than the originally described 70 kDa size exclusion limit, suggesting that virions could also “fit” within the conduits if they gained access. Consistent with these studies, we show that conditional deletion of PLVAP specifically on LECs also allowed much larger numbers of virions to enter the conduits.

The simplest explanation for entry is that the LEC PVLAP “sieve” is leaky, allowing a few molecules to pass through, especially when present at high concentration. As detailed ultrastructural studies of the LN mapping all conduit entry points have not been performed, it is unknown if the structures made by PLVAP guard all or only a subset of LN conduits. Likewise, it remains possible that a limited number of sinus-borne virions could gain access

to the conduit system, bypassing PLVAP. Evolutionarily, allowing a few virions to circumvent the sieve might make sense, as this would allow for rapid, paracortical T cell priming without the risk of large-scale pathogen escape or complete paracortical infection. Recent studies have demonstrated that larger molecules (still much smaller than virions) can be accommodated by the conduit system if injected directly into the paracortex of the LN [8]. Thus, the rate-limiting step for virion transport is likely conduit entry, and it will be important to determine the mechanisms underlying access.

In summary, our study demonstrates the delivery of virions to the LN paracortex by conduits. This newly uncovered route of nodal antigen transport should prove informative for vaccine design, in particular for live-viral or complexed-mRNA vaccines that can replicate small numbers of conduit-delivered antigen in paracortical APCs.

METHODS

Mice

Specific pathogen-free C57BL/6, B6(Cg)-Tyrc-2J/J, and *Ifnar*$^{-/-}$ mice were obtained from Taconic Farms. STOCK Tg (CAG-DsRed*MST) 1Nagy/J mice were crossed to OT-I TCR transgenic mice (NIAID Intramural Research Repository) and bred for homozygosity to create DsRed OT-I mice. *Plvap*$^{fl/fl}$ mice [29] on C57BL/6J background were crossed to *Prox1*-CreERT2$^{tg/+}$ mice [51] to create PLVAP^{iLECKO} mice (genotype: *Plvap*$^{fl/fl}$ *Prox1*-CreERT2$^{tg/+}$). *Prox1*-CreERT2$^{tg/+}$ mice on C57BL/6 genetic background were a kind gift from G. Oliver (U Chicago). *Plvap*^{iLECKO} and littermate *Plvap*$^{fl/fl}$ control mice were bred in house at Dartmouth and shipped to NIH. 6- to 16-week-old female mice were used in all experiments unless otherwise noted. Mice were housed under specific pathogen-free conditions (including murine norovirus, mouse parvovirus, and mouse hepatitis virus) and maintained on standard rodent chow and water supplied *ad libitum*. All animal studies were approved by and performed in accordance with the Animal Care and Use Committee of the National Institute of Allergy and Infectious Diseases.

Tamoxifen administration

For tamoxifen treatment, 2 mg/mouse was administered intraperitoneally every other day for two weeks prior to infection.

T cell transfers

Spleens and nodes from OT-I dsRed mice were purified to >90% purity using an Automacs (Miltenyi Biotech) using a CD8^{+} T cell negative selection kit. At least one day prior to infection, 2.5×10^5 (unless otherwise indicated) OT-I cells were transferred intravenously.

Viruses and infections

Mice were infected via footpad using an insulin syringe and injected the specified doses of VACV or MVA from purified stocks (in a total volume of 10 μls) into wild-type C57Bl/6 animals. VACVs used in this study were VV-NP-S-GFP, MVA-NP-S-GFP, and VACV-NP-eGFP (an identical virus lacking the SIINFEKL determinant). All viruses have been previously described and virus stocks were grown and titered in house, as described [10, 52].

ZIKV was grown and tittered in Vero cells. 10^4 FFU of 10^4 pfu of ZIKV H/PF/2013 was inoculated footpad in 10 μls into *Ifnar*$^{-/-}$ mice.

Alexa-647 labeled virus was prepared with sucrose-purified virus and a Protein Labeling Kit (ThermoFisher) according to the manufacturer's instructions. Labeled virus was purified twice through a spin column to remove free dye and then by sucrose gradient. Gold-labeled VACV was prepared using purified virus and a was conjugated to 10 nm gold nanoparticle conjugation kit (InnovaCoat GOLD, Innova Biosciences). Virus and reaction buffer were mixed according to the manufacturer's instructions and the mixture was used to reconstitute InnovaCoat GOLD particles. The reaction mixture was incubated at room temperature for 15 min, quenched for 5 min at 25 °C, spun down and resuspended in 1mM TRIS pH 9.0 buffer prior to injection.

Flow cytometric analysis of T cell activation

Single cell suspensions of popliteal lymph nodes were prepared by homogenization in Kontes pestle tubes prior to filtration through 70 μm nylon cell strainers. Cells were stained with the following antibodies: CD45 (clone 30-F11, eBioscience, Lot#E10032–1635); CD8α (clone 53–6.7, eBioscience, many different lots); CD69 (clone H1.2F3, eBioscience, Lot#B207773); and IFN-γ (clone XMG1.2, eBioscience, Lot#E024667). Cells were analyzed on an LSR II flow cytometer (BD Biosciences) using FacsDiva software, and resultant data analyzed using FlowJo (Treestar).

Confocal microscopy of frozen LN sections

Popliteal lymph nodes were removed at the indicated times, fixed overnight in periodate-lysine-paraformaldehyde buffer, and placed in 30% sucrose/PBS for 24 h before embedding in optimal-cutting-temperature medium (Electron Microscopy Sciences) and freezing in dry-ice-cooled isopentane. Eighteen-micron sections were cut on a Leica cryostat (Leica Microsystems). Sections were blocked with 5% goat, donkey, bovine, rat or rabbit serum and then stained with one or more of the following Abs: CD11b (clone M1/70, eBioscience, Lot#E022424, E15525–01, 4319572, or B259438); CD11c (clone N418, eBioscience, Lot#4288340, 4339477, or E029528); CD205 (clone NLDC-145, Biolegend, Lot#B251007); B220 (clone RA3–6B2, eBioscience, Lot#4288340, 4339477, or 4306068); CD8α (clone 53–6.7, eBioscience, many different lots); Lyve-1 (clone ALY7, eBioscience, Lot#4291625 or 4311240); ERTR7 (staining a fibroblastic reticular cell antigen and used to identify the LN stromal network including conduits, blood vessels and lymphatic sinuses; rat monoclonal, Abcam (cat#51824); CD69 (polyclonal goat, R&D Systems, Cat#AF2386, Lot 0117021 or 0107081); anti-GFP (polyclonal, eBioscience, Lot#E051981634); anti-vaccinia virus (Accurate Chemical Group, Lot#J2368); anti-NS2B (Genetex, Lot#42508); and/or Lyve-1 (clone ALY7, eBioscience, Lot#4291625, 4311240 or 1978147). Sections were incubated with secondary antibodies as needed and as controls, and images were acquired using identical PMT (photomultiplier tube) and laser settings. In some instances, Huygens Essentials was used to deconvolve confocal images.

Confocal tile scans

Scans were taken of an entire popliteal LN section equaling a 7 mm^2 imaged area and individual fields (tiles) were merged into one image.

Image analysis

Images were analyzed using Imaris software (Bitplane). LN regions (SCS/IFA, T cell zone, Medulla, and B cell follicles) were classified using Lyve-1, B220, and ERTR7 staining as described in [18]. GFP^+ infected cells and OT-I $CD8^+$ T cells were identified using the spot detection algorithm of Imaris and manually assigned to LN regions.

For analyses of infected cells touching conduits or sinuses, images were processed with Imaris software and a 2-dimensional projection of the lymph node slices was exported from this software for further analysis with CellProfiler, an open source software package available from the Broad Institute at www.cellprofiler.org. Image analysis then relied on the separation of fluorescent channels between $ERTR7^+$ (conduit and sinus) and $Lyve\text{-}1^+$ (sinus) tissues versus GFP^+ (virus-infected) cells. Classification of these structures was achieved using an Otsu thresholding algorithm with two classes. In each image, objects (either cells or tissue structures) were then identified using CellProfiler provided functions, and infected cells (containing nuclearly localized fluorescence due to the karyophilic properties of the GFP fusion protein expressed [10]) identified within 10 microns of conduits or sinuses were classified as neighbors of either one, both, or neither signal. This method of analysis was verified through a by-hand counting of 4 lymph node tile scans by two separate individuals, with a strong correlation (R^2 =.948) between computer identified virus count and by-hand identified virus count.

For T cell activation analysis on lymph node sections, tile scans were taken with nodes stained with ERTR7, B220, and polyclonal anti-CD69 as described above. For calculation of the percentage of activated OT-I $CD8^+$ T cells, dsRed OT-I cells were detected using the spot algorithm of Imaris and the mean fluorescent intensity of the CD69 channel was determined for each individual spot. Spots with a mean fluorescent intensity of 50 or greater were considered activated T cells and used to calculate the total percentage activated. Spots were then filtered to exclude those with a fluorescent mean intensity < 50, and then manually assigned a LN region. Where indicated, exclusion of non-activated cells was not performed (all T cells are shown).

Electron microscopy of LN sections

Popliteal lymph nodes were fixed in 2% glutaraldehyde/0.1M sodium cacodylate pH?? buffer, washed in 0.1M sodium cacodylate buffer, post-fixed with 1% osmium tetroxide, and washed in buffer. The nodes were then incubated in 1% aqueous tannic acid, washed in distilled, sterile water and incubated with 2% aqueous uranyl acetate overnight and washed in water the next morning. The samples were dehydrated in a series of ethyl alcohol: 50%, 70%, 90%, 100% and then propylene oxide. The nodes were embedded in Embed 812 and sections were cut on a Leica EM UC7 ultramicrotome (Leica Microsystems Inc.). Thin sections were post-stained with 7% uranyl acetate in 50% ethanol and then 0.01% lead citrate. Sections were reviewed for conduits in the paracortex of the LN and identified

conduits were scanned for the presence of virions. Identified virions were photographed on the Tecnai G2 Spirit transmission electron microscope (FEI/Thermo Fisher Scientific) fitted with a Gatan Orius CCD camera (Gatan, Inc.) and a FEI Eagle camera. Chemicals were purchased from Electron Microscopy Sciences (EMS).

Statistical analyses

Significances were calculated using GraphPad (Prism) using unpaired two-tailed Student's *t* test.

Data availability statement

The data that support the findings of this study are available from the corresponding author upon reasonable request.

Supplementary Material

Refer to Web version on PubMed Central for supplementary material.

Acknowledgments

This work was supported by the Intramural Research Program of NIAID, NIH (H.D.H.). R.V.S. was supported by NIH grants R21CA172983, R21CA175592, R01GM120592 and AHA 16GRNT27260362. We thank K. Dowd and T. Pierson (Viral Pathogenesis Section, Laboratory of Viral Diseases, NIAID) for assistance with ZIKV infection and J. Kabat (Biological Imaging Section, NIAID) for assistance with microscopic image analysis. G. Oliver (University of Chicago) provided *Prox1*-CreERT2$^{tg/+}$ mice on C57BL/6 genetic background.

References

1. Gretz JE, Norbury CC, Anderson AO, Proudfoot AE & Shaw S Lymph-borne chemokines and other low molecular weight molecules reach high endothelial venules via specialized conduits while a functional barrier limits access to the lymphocyte microenvironments in lymph node cortex. J Exp Med 192, 1425–1440 (2000). [PubMed: 11085745]
2. Itano AA et al. Distinct dendritic cell populations sequentially present antigen to CD4 T cells and stimulate different aspects of cell-mediated immunity. Immunity 19, 47–57 (2003). [PubMed: 12871638]
3. Sixt M et al. The conduit system transports soluble antigens from the afferent lymph to resident dendritic cells in the T cell area of the lymph node. Immunity 22, 19–29 (2005). [PubMed: 15664156]
4. Pape KA, Catron DM, Itano AA & Jenkins MK The humoral immune response is initiated in lymph nodes by B cells that acquire soluble antigen directly in the follicles. Immunity 26, 491–502 (2007). [PubMed: 17379546]
5. Gerner MY, Torabi-Parizi P & Germain RN Strategically localized dendritic cells promote rapid T cell responses to lymph-borne particulate antigens. Immunity 42, 172–185 (2015). [PubMed: 25607462]
6. Rantakari P et al. The endothelial protein PLVAP in lymphatics controls the entry of lymphocytes and antigens into lymph nodes. Nat Immunol 16, 386–396 (2015). [PubMed: 25665101]
7. Gerner MY, Casey KA, Kastenmuller W & Germain RN Dendritic cell and antigen dispersal landscapes regulate T cell immunity. J Exp Med 214, 3105–3122 (2017). [PubMed: 28847868]
8. Thierry GR et al. The conduit system exports locally secreted IgM from lymph nodes. J Exp Med 215, 2972–2983 (2018). [PubMed: 30429248]
9. Norbury CC, Malide D, Gibbs JS, Bennink JR & Yewdell JW Visualizing priming of virus-specific CD8+ T cells by infected dendritic cells in vivo. Nature immunology 3, 265–271 (2002). [PubMed: 11828323]

10. Hickman HD et al. Direct priming of antiviral CD8+ T cells in the peripheral interfollicular region of lymph nodes. Nature immunology 9, 155–165 (2008). [PubMed: 18193049]
11. Kastenmuller W, Torabi-Parizi P, Subramanian N, Lammermann T & Germain RN A spatially-organized multicellular innate immune response in lymph nodes limits systemic pathogen spread. Cell 150, 1235–1248 (2012). [PubMed: 22980983]
12. Kastenmuller W et al. Peripheral prepositioning and local CXCL9 chemokine-mediated guidance orchestrate rapid memory CD8+ T cell responses in the lymph node. Immunity 38, 502–513 (2013). [PubMed: 23352234]
13. Gaya M et al. Host response. Inflammation-induced disruption of SCS macrophages impairs B cell responses to secondary infection. Science 347, 667–672 (2015). [PubMed: 25657250]
14. Sagoo P et al. In vivo imaging of inflammasome activation reveals a subcapsular macrophage burst response that mobilizes innate and adaptive immunity. Nat Med 22, 64–71 (2016). [PubMed: 26692332]
15. Brewitz A et al. CD8+ T Cells Orchestrate pDC-XCR1+ Dendritic Cell Spatial and Functional Cooperativity to Optimize Priming. Immunity 46, 205–219 (2017). [PubMed: 28190711]
16. Junt T et al. Subcapsular sinus macrophages in lymph nodes clear lymph-borne viruses and present them to antiviral B cells. Nature 450, 110–114 (2007). [PubMed: 17934446]
17. Iannacone M et al. Subcapsular sinus macrophages prevent CNS invasion on peripheral infection with a neurotropic virus. Nature 465, 1079–1083 (2010). [PubMed: 20577213]
18. Sung JH et al. Chemokine guidance of central memory T cells is critical for antiviral recall responses in lymph nodes. Cell 150, 1249–1263 (2012). [PubMed: 22980984]
19. Hickman HD et al. Chemokines control naive CD8+ T cell selection of optimal lymph node antigen presenting cells. The Journal of experimental medicine 208, 2511–2524 (2011). [PubMed: 22042976]
20. Woodruff MC et al. Trans-nodal migration of resident dendritic cells into medullary interfollicular regions initiates immunity to influenza vaccine. J Exp Med 211, 1611–1621 (2014). [PubMed: 25049334]
21. Palframan RT et al. Inflammatory chemokine transport and presentation in HEV: a remote control mechanism for monocyte recruitment to lymph nodes in inflamed tissues. J Exp Med 194, 1361–1373 (2001). [PubMed: 11696600]
22. Katakai T et al. A novel reticular stromal structure in lymph node cortex: an immuno-platform for interactions among dendritic cells, T cells and B cells. Int Immunol 16, 1133–1142 (2004). [PubMed: 15237106]
23. Bajenoff M & Germain RN B-cell follicle development remodels the conduit system and allows soluble antigen delivery to follicular dendritic cells. Blood 114, 4989–4997 (2009). [PubMed: 19713459]
24. Moss B Poxviridae: the viruses and their replication In: Knipe D.M.a.H., P.M (ed). Fields Virology. Lippincott-Raven, 2001, pp 2849–2884.
25. Moss B et al. Host range restricted, non-replicating vaccinia virus vectors as vaccine candidates. Adv Exp Med Biol 397, 7–13 (1996). [PubMed: 8718576]
26. Pierson TC & Diamond MS The emergence of Zika virus and its new clinical syndromes. Nature 560, 573–581 (2018). [PubMed: 30158602]
27. Baden LR et al. First-in-Human Randomized, Controlled Trial of Mosaic HIV-1 Immunogens Delivered via a Modified Vaccinia Ankara Vector. J Infect Dis 218, 633–644 (2018). [PubMed: 29669026]
28. La Rosa C et al. MVA vaccine encoding CMV antigens safely induces durable expansion of CMV-specific T cells in healthy adults. Blood 129, 114–125 (2017). [PubMed: 27760761]
29. Stan RV et al. The diaphragms of fenestrated endothelia: gatekeepers of vascular permeability and blood composition. Dev Cell 23, 1203–1218 (2012). [PubMed: 23237953]
30. Sirohi D et al. The 3.8 A resolution cryo-EM structure of Zika virus. Science 352, 467–470 (2016). [PubMed: 27033547]
31. Hogquist KA et al. T cell receptor antagonist peptides induce positive selection. Cell 76, 17–27 (1994). [PubMed: 8287475]

32. Hickman HD et al. CXCR3 chemokine receptor enables local CD8(+) T cell migration for the destruction of virus-infected cells. Immunity 42, 524–537 (2015). [PubMed: 25769612]
33. Hildner K et al. Batf3 deficiency reveals a critical role for CD8alpha+ dendritic cells in cytotoxic T cell immunity. Science 322, 1097–1100 (2008). [PubMed: 19008445]
34. Belz GT et al. Cutting edge: conventional CD8 alpha+ dendritic cells are generally involved in priming CTL immunity to viruses. J Immunol 172, 1996–2000 (2004). [PubMed: 14764661]
35. Gerner MY, Kastenmuller W, Ifrim I, Kabat J & Germain RN Histo-cytometry: a method for highly multiplex quantitative tissue imaging analysis applied to dendritic cell subset microanatomy in lymph nodes. Immunity 37, 364–376 (2012). [PubMed: 22863836]
36. Link A et al. Fibroblastic reticular cells in lymph nodes regulate the homeostasis of naive T cells. Nat Immunol 8, 1255–1265 (2007). [PubMed: 17893676]
37. Denton AE, Roberts EW, Linterman MA & Fearon DT Fibroblastic reticular cells of the lymph node are required for retention of resting but not activated CD8+ T cells. Proc Natl Acad Sci U S A 111, 12139–12144 (2014). [PubMed: 25092322]
38. Cremasco V et al. B cell homeostasis and follicle confines are governed by fibroblastic reticular cells. Nat Immunol 15, 973–981 (2014). [PubMed: 25151489]
39. Bajenoff M et al. Stromal cell networks regulate lymphocyte entry, migration, and territoriality in lymph nodes. Immunity 25, 989–1001 (2006). [PubMed: 17112751]
40. Acton SE et al. Dendritic cells control fibroblastic reticular network tension and lymph node expansion. Nature 514, 498–502 (2014). [PubMed: 25341788]
41. Astarita JL et al. The CLEC-2-podoplanin axis controls the contractility of fibroblastic reticular cells and lymph node microarchitecture. Nat Immunol 16, 75–84 (2015). [PubMed: 25347465]
42. Yang CY et al. Trapping of naive lymphocytes triggers rapid growth and remodeling of the fibroblast network in reactive murine lymph nodes. Proc Natl Acad Sci U S A 111, E109–118 (2014). [PubMed: 24367096]
43. Estes JD Pathobiology of HIV/SIV-associated changes in secondary lymphoid tissues. Immunol Rev 254, 65–77 (2013). [PubMed: 23772615]
44. Mueller SN et al. Viral targeting of fibroblastic reticular cells contributes to immunosuppression and persistence during chronic infection. Proc Natl Acad Sci U S A 104, 15430–15435 (2007). [PubMed: 17878315]
45. Ng CT, Nayak BP, Schmedt C & Oldstone MB Immortalized clones of fibroblastic reticular cells activate virus-specific T cells during virus infection. Proc Natl Acad Sci U S A 109, 7823–7828 (2012). [PubMed: 22550183]
46. Scandella E et al. Restoration of lymphoid organ integrity through the interaction of lymphoid tissue-inducer cells with stroma of the T cell zone. Nat Immunol 9, 667–675 (2008). [PubMed: 18425132]
47. Davis KJ et al. Pathology of experimental Ebola virus infection in African green monkeys. Involvement of fibroblastic reticular cells. Arch Pathol Lab Med 121, 805–819 (1997). [PubMed: 9278608]
48. Steele KE, Anderson AO & Mohamadzadeh M Fibroblastic reticular cell infection by hemorrhagic fever viruses. Immunotherapy 1, 187–197 (2009). [PubMed: 20635940]
49. Steele KE, Anderson AO & Mohamadzadeh M Fibroblastic reticular cells and their role in viral hemorrhagic fevers. Expert Rev Anti Infect Ther 7, 423–435 (2009). [PubMed: 19400762]
50. Twenhafel NA et al. Pathology of experimental aerosol Zaire ebolavirus infection in rhesus macaques. Vet Pathol 50, 514–529 (2013). [PubMed: 23262834]
51. Srinivasan RS et al. Lineage tracing demonstrates the venous origin of the mammalian lymphatic vasculature. Genes Dev 21, 2422–2432 (2007). [PubMed: 17908929]
52. Hickman HD et al. Anatomically restricted synergistic antiviral activities of innate and adaptive immune cells in the skin. Cell host & microbe 13, 155–168 (2013). [PubMed: 23414756]

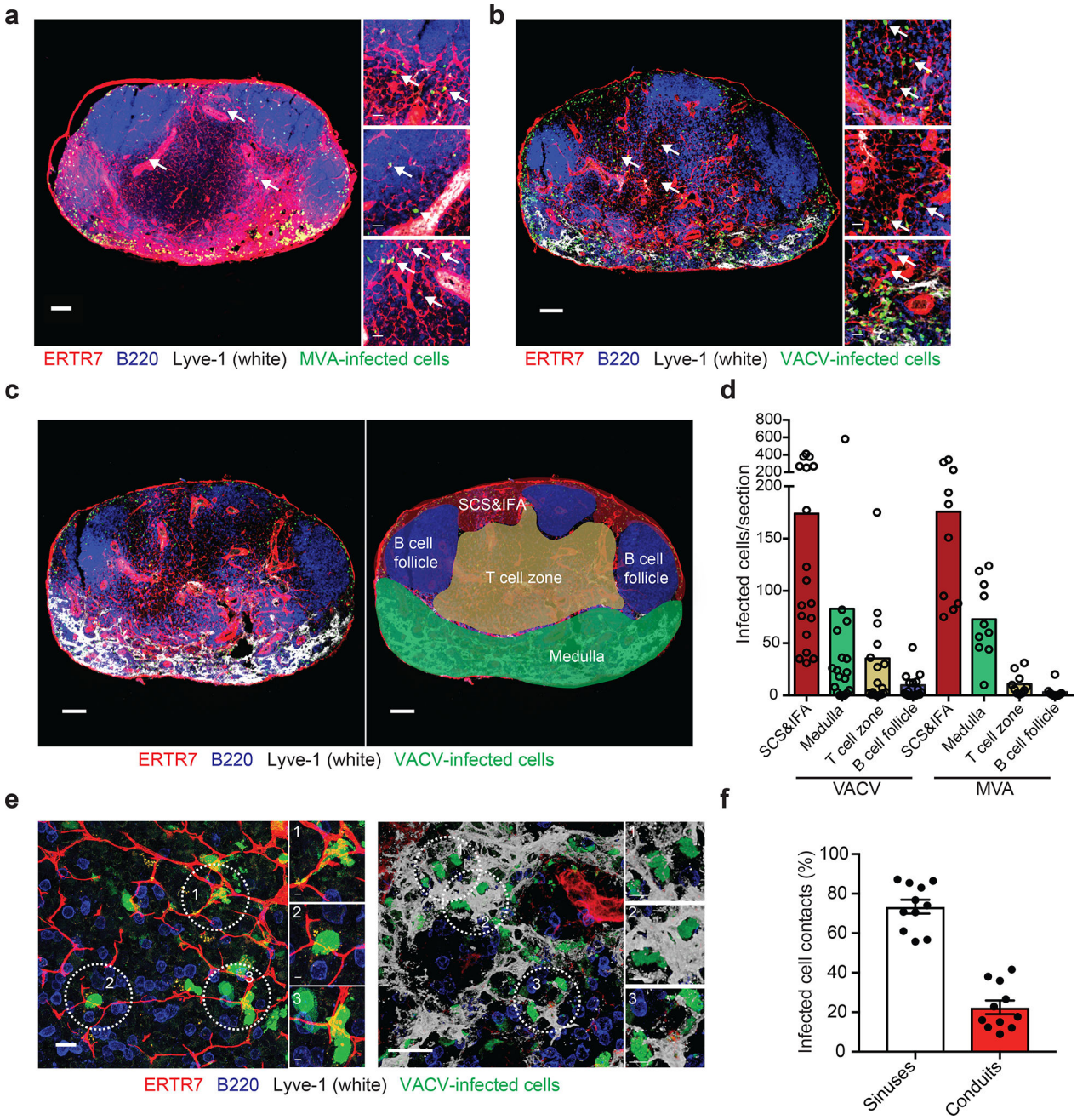

Figure 1. VACV and MVA rapidly infect T cell-zone cells associated with conduits.

a-b) Maximum intensity projections (MIP) of sections of popliteal LNs harvested 8 h after footpad injection 10^8 pfu of MVA (a) or VACV (b). ERTR7 = red (labeling conduits and blood vessels), Lyve-1 (labeling non-conduit lymphatic sinuses) = white, MVA or VACV-infected cells = green nuclear signal, B220 (labeling B cells) = blue. Arrows point to some of the virus-infected cells associated with conduits. Scalebar = 100 μm. Higher magnification images are shown to the right. Scalebars = 20 μm. (n =18 LN sections for VACV; 10 LN sections for MVA taken over 4–6 independent experiments) **c**) Schematic for assignment of LN regions into subcapsular sinus and interfollicular area region (SCS&IFA),

B cell follicles, T cell zone, and medulla. Left = LN as stained in (a) and (b), right with areas overlaid. Scalebars = 100 μm. **d**) Quantitation of infected cells (either MVA or VACV) per LN section 8 h post-infection from sections in (a-b). Dots represent individual sections. Bars = mean. **e**) High magnification images showing the association of T cell-zone infected cells (green, nuclear) with conduits (red, left); or medullary infected cells associated with lymphatic sinuses (white, right). Scalebars = 20 μm. Individual infected cells that are highlighted in circles are shown in higher magnification on the right for each image. Scalebars = 3 μm (right insets) and 5 μm (left insets). **f**) Quantitation of the percentage of infected cells contacting either lymphatic endothelial cells (of LN sinuses) or conduits in the VACV sections (n=11, 3 independent experiments). Bars show mean. Scalebars = SEM.

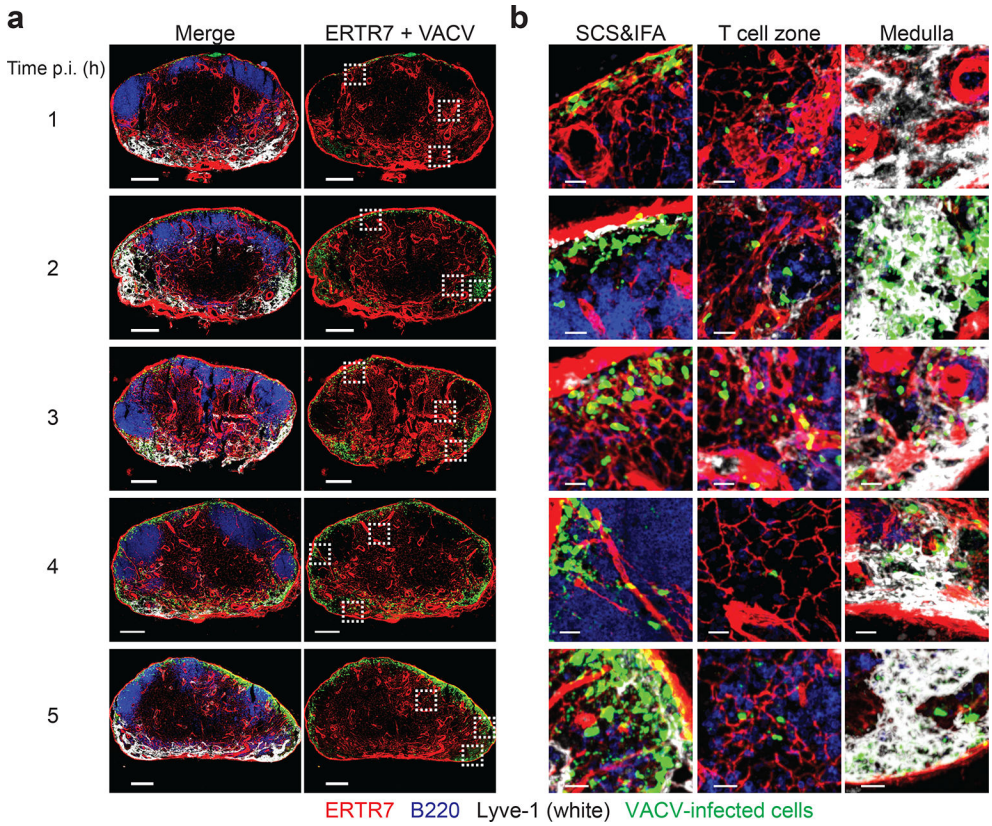

Figure 2. Conduit-associated VACV-infected cells can be visualized in the LN within an h of infection.

a) Maximum intensity projections (MIP) of sections of popliteal LNs harvested at the indicated h post infection with 10^8 pfu of VACV (time indicated on the left). ERTR7 = red (labeling conduits and blood vessels), Lyve-1 (labeling non-conduit lymphatic sinuses) = white, VACV-infected cells = green nuclear signal, B220 (labeling B cells) = blue. Dashed boxes indicate areas of the LN section with magnified views shown in (b). Scalebars = 200 μm. Results are representative of 6 LNs from 3 different experiments. **b**) Higher magnification images of LN sections in (a) showing VACV-infected cells in the SCS and IFA region, T cell zone and medulla at the indicated time post-infection (far left). Scalebars = 20 μm.

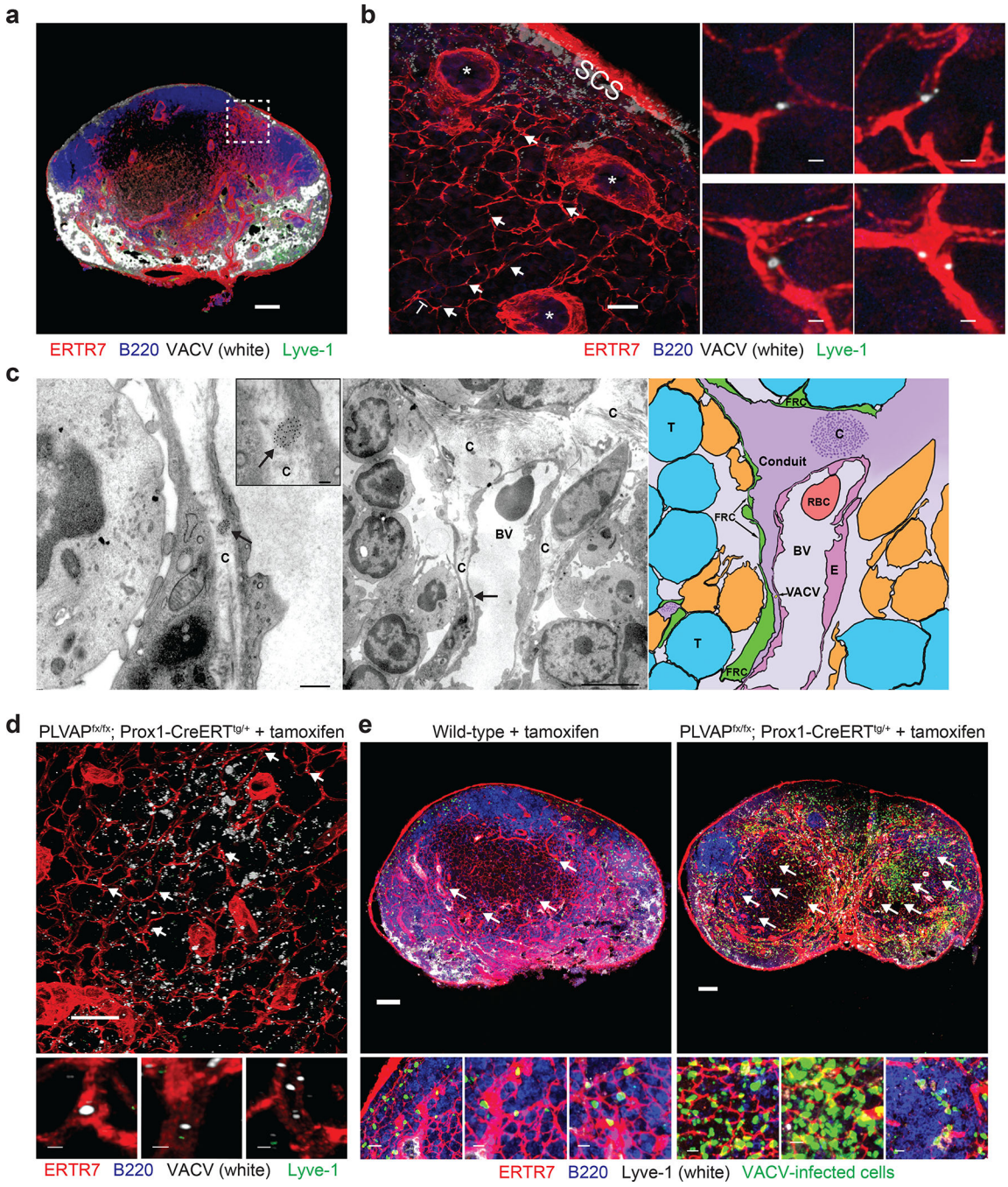

Figure 3. VACV virions can be transported in LN conduits.

a) Maximum intensity projection (MIP) of a popliteal LN section harvested 3 m after footpad injection of purified Alexa 647-labeled VACV (white) showing labeled virus in subcapsular and medullary sinuses (green). ERTR7 = red (labeling conduits and blood vessels), Lyve-1 (labeling non-conduit lymphatic sinuses) = green, Alexa 647-labeled VACV = white, B220 (B cells) = blue. The area shown in the dashed box is magnified in b). Scalebar = 100 μm. **b**) Blended projection of the boxed area of (a). Arrows point to some examples of labeled virions in conduits. Scalebar = 50 μm. * denote blood vessels. T = T

cell zone. SCS = subcapsular sinus. Right panels show magnified images. Scalebar = 1 μm. Images in (a,b) are representative of 10 LNs taken in 4 separate experiments. **c**) Electron micrographs of popliteal LN harvested 5 m after footpad injection of 10 nm-gold-particle-conjugated VACV. Left panel) VACV virion in a conduit (labeled with a C) is indicated by an arrow. Scalebar = 500 nm. Inset shows a higher magnification of virion. Scalebar = 100 nm. Middle panel) Lower magnification of area in right panel showing typical down-spout like conduit (C) in the node. An arrow indicates the location of the virion. BV= blood vessel. Scalebar = 5 μm. Right panel) schematic of the image in the middle panel showing the VACV virion (gold) in the conduit (purple). Arrow indicates the location of the virion. The conduit is labeled “conduit”, T = T cell, FRC = fibroblastic reticular cell, RBC = red blood cell, E = endothelial cell, BV = blood vessel. An area of the conduit with collagen fibers running transverse to the LN section is indicated with a “C”. Results are indicative of 14 grids from 2 separate experiments. **d**) Alexa 647-labeled virus was injected footpad into tamoxifen-treated $PLVAP^{iLECKO}$ (genotype $PLVAP^{fx/fx}$; Prox1-$CreERT2^{tg/+}$) mice (depleting PLVAP on lymphatic endothelial cells (LECs)). ERTR7 = red (labeling conduits and blood vessels), Lyve-1 (labeling non-conduit lymphatic sinuses) = green, Alexa 647-labeled VACV = white, B220 (B cells) = blue. Arrows indicate some examples of labeled virus in conduits. Scalebar = 100 μm. Higher magnification images are shown in the insets below the image. Scalebar = 1 μm. Results are representative of 6 mice and 3 experiments. **e**) MIPs of sections of popliteal LN harvested 8 h post-footpad infection of wild-type mice treated with tamoxifen (left), or of transgenic animals with *Plvap* conditionally ablated in LECs (right). Arrows indicate some examples of virus-infected cells (green) in the T cell zone. Scalebars = 100 μm. Higher magnification images are shown below each node. Scalebars = 10 μm. ERTR7 = red (labeling conduits and blood vessels), Lyve-1 (labeling non-conduit lymphatic sinuses) = white, VACV-infected cells = green nuclear signal, B220 (labeling B cells) = blue. Results are representative of 9 mice and 3 experiments.

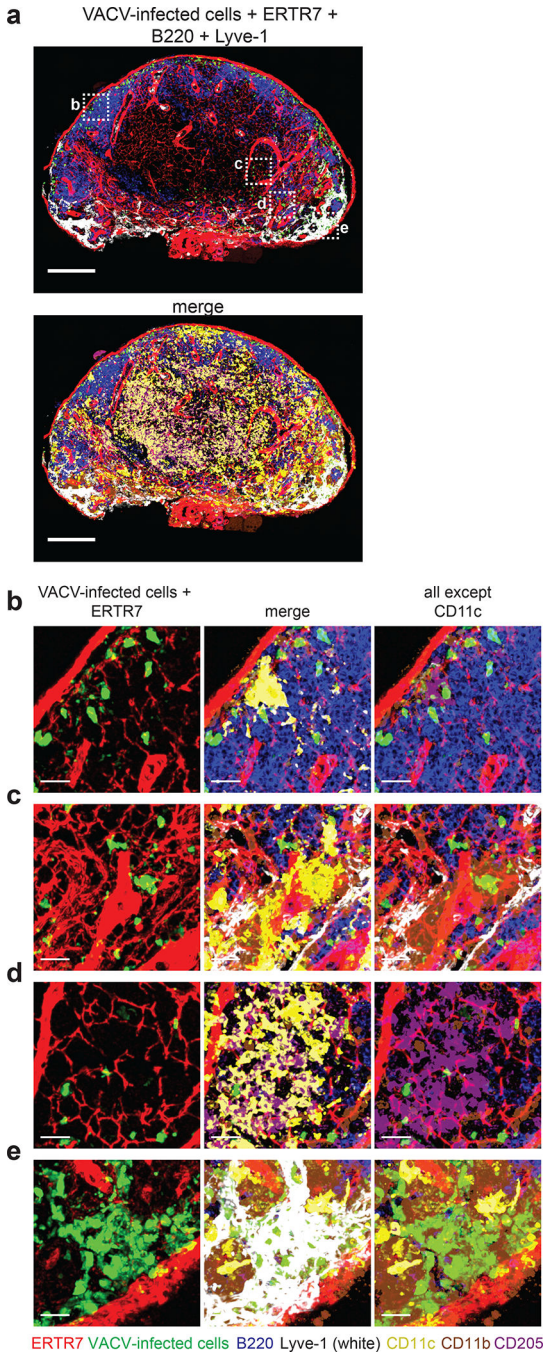

Figure 4. VACV infects conduit-associated dendritic cells.

a) Maximum intensity projection (MIP) of a section of a popliteal LN harvested 8 h after footpad injection of 10^8 pfu of VACV. Top panel) staining as in previous figures showing ERTR7 = red (labeling conduits and blood vessels), Lyve-1 (labeling non-conduit lymphatic sinuses) = white, VACV-infected cells = green nuclear signal, B220 (labeling B cells) = blue. Bottom panel) same image as the top adding staining for CD11c = yellow, CD205 = purple, and CD11b = brown. Scalebars = 200 μm. **b-e**) High magnification images of dashed boxes in (a) showing **b**) an infected $CD205^+$ DC in the SCS, **c**) an infected $CD11b^+$ DC near a

lymphoid sinus, **d**) infected $CD205^+$ DCs associated with conduits in the T cell zone, **e**) infected $CD11b^+$ macrophages in the medullary sinus. Scalebars = 20 μm. Results are representative of 10 LNs and 4 experiments.

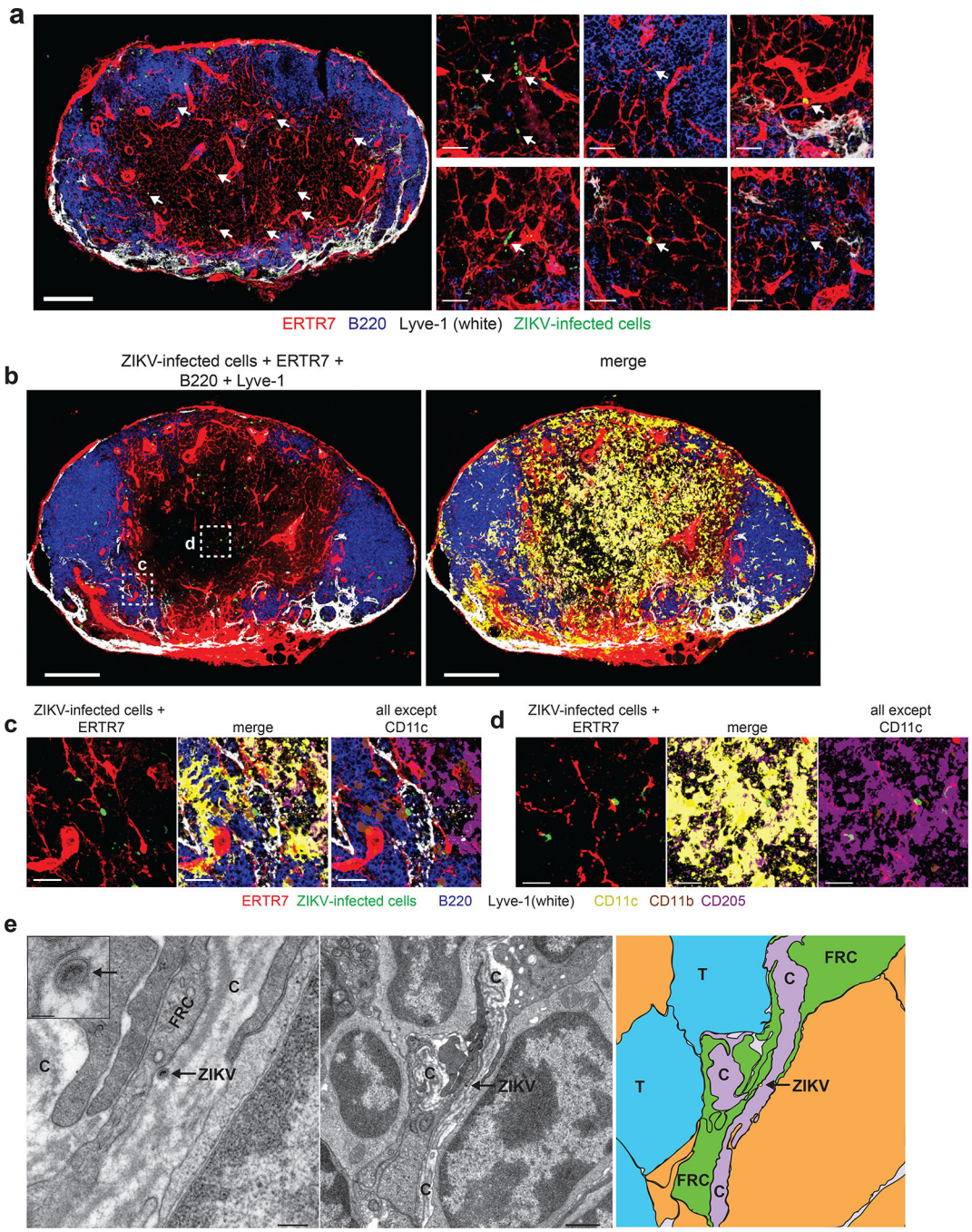

Figure 5. Zika virions are also transported by conduits.

a) Maximum intensity projection (MIP) of a section of a popliteal LN harvested 24 h after footpad injection of 10^4 FFU ZIKV. Arrows indicate ZIKV-infected cells (green, stained for ZIKV NS2B protein) associated with conduits. ERTR7 = red (labeling conduits and blood vessels), Lyve-1 (labeling non-conduit lymphatic sinuses) = white, B220 (labeling B cells) = blue. Scalebar = 200 μm. Smaller panels to the left show higher magnification images. Scalebars = 20 μm. Images are representative of 20 LNs from 5 experiments. **b**) Maximum intensity projection (MIP) of a section of a popliteal LN harvested 24 h after footpad

injection of 10^4 FFU ZIKV. Left panel is stained as in (a). Right panel adds on staining for CD11c = yellow, CD205 = purple, and CD11b = brown. Scalebars = 200 μm. **c-d**) High magnification images of dashed boxes in (b) showing **c**) an infected $CD11b^+$ DC in a sinus (white), and **d**) an infected $CD205^+$ DC in the T cell zone. Scalebars = 20 μm. Results are indicative of 10 LNs from 3 experiments. **e**) Electron micrographs of popliteal LN harvested 24 h after footpad injection of 10^4 FFU ZIKV. Left panel) ZIKV virion is indicated in an arrow in a conduit (labeled with a C). Scalebar = 200 nm. Inset shows a higher magnification of virion. Scalebar = 50 nm. FRC = fibroblastic reticular cell. Middle panel) lower magnification image of left panel. Scalebar = 1 μm. Right panel) schematic of the image in the middle panel showing the ZIKV virion (yellow) in the conduit (purple). Arrow indicates the location of the virion. Conduit = C, T = T cell, FRC = fibroblastic reticular cell. 24 grids from 6 nodes and 3 experiments were analyzed.

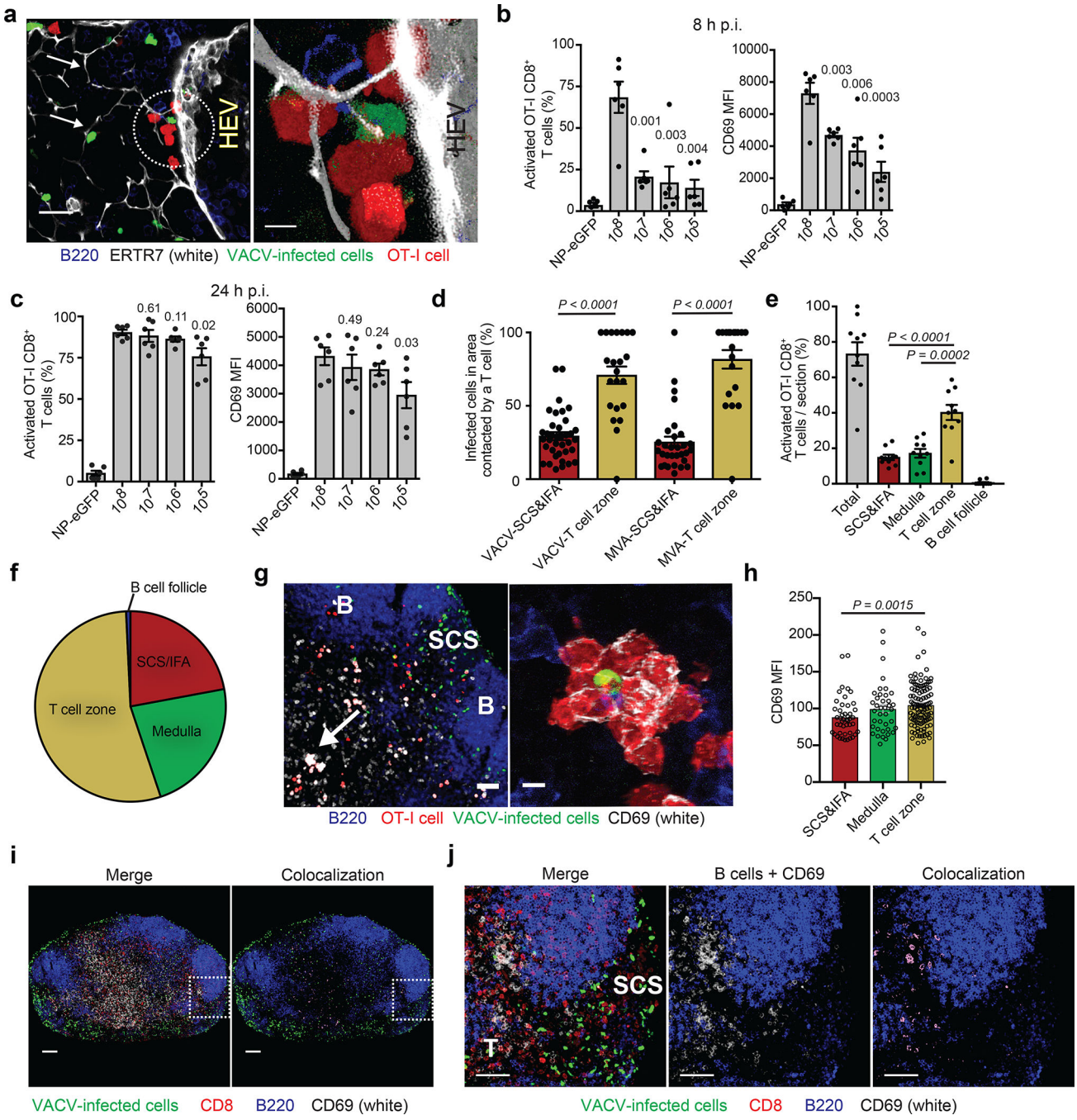

Figure 6. CD8$^+$ T cells are rapidly activated by virus in the T cell zone.

a) Blended projections of T cells (red) clustered around a conduit (white)-associated VACV-infected cell (green) near a high endothelial venule (HEV, indicated in picture). Arrows point to conduits. Scalebar = 20 μm. Area in circle is magnified on the right. Scalebar = 5 μm. ERTR7= white, VACV-infected cells = green, OT-I CD8$^+$ T cells = red, B220 = blue. Results are representative of 30 LN sections taken from 5 experiments. **b**) OT-I CD8$^+$ T cell activation as determined by flow cytometry of single-cell suspensions of popliteal LNs harvested 8 h p.i. 10^6 OT-I cells were transferred 12–24 h prior to infection. NP-eGFP (no

SIINFEKL) was given at 10^7 pfu; all other infections used NP-S-eGFP (containing SIINFEKL) at the indicated dose. Activation was determined by CD69 expression. MFI is shown on the right. Dots = individual LNs. n = 6. Results were repeated 3 times with 3–6 mice/group. Bars = mean. Error bars = SEM. **c**) OT-I $CD8^+$ T cell activation in (b) but 24 h p.i. Dots = individual LNs. n = 6. Results were repeated 3 times with 3–6 mice/group. Bars = mean. Error bars = SEM. **d**) Quantitation of the percentage of VACV- or MVA-infected cells in either the SCS and IFA region or T cell zone contacted by OT-I $CD8^+$ T cells (n = 37 VACV or 32 MVA; dots indicate individual sections). Bars = mean. Error bars = SEM. **e**) Percentage of activated OT-I $CD8^+$ T cells (those with CD69 MFI > 50) in each region of 10 LN sections harvested 8 h after infection with 10^8 pfu VACV. Percentages shown are activated cells/total cells in each region. Dots = individual LN sections. Bars = mean. Error bars = SEM. **f**) Percentage of only the activated OT-I $CD8^+$ T cells (as opposed to total cells in (e)) found in each LN region. **g**) MIP LN section 8 h p.i. showing OT-I $CD8^+$ T cell activation. B = B cell follicle, SCS = subcapsular sinus. Arrow indicates activated T cell cluster in the T cell zone, magnified on the right. Scalebars = 50 μm, left and 5 μm, right. OT-I $CD8^+$ T cells = red, CD69 = white, VACV-infected cells = green, B220 = blue. **h**) MFI of CD69 on all activated cells in each region of the popliteal LN shown in (g). n =197 T cells. Bars = mean. Error bars = SEM. **i**) MIP of popliteal LN harvested 8 h post infection with 10^8 pfu VACV (green) without OT-I transfer. Endogenous, polyclonal $CD8^+$ T cells = red. Colocalization of polyclonal $CD8^+$ T cell signal (red) and CD69 (white) signal is shown in purple. B220 = blue, VACV-infected cells = green. The boxed area is magnified in (j). scalebars = 100 μm **j**) Higher magnification MIP image of (i) showing both the SCS&IFA (labeled SCS) and T cell zone (T). Colocalization of polyclonal $CD8^+$ T cell signal (red) and CD69 (white) signal is shown in purple. scalebars = 50 μm. f,h,i,j) 6 LNs from 3 experiments were analyzed. g) 10 LNs from 5 experiments were analyzed. Statistics = unpaired two-tailed *t* test.

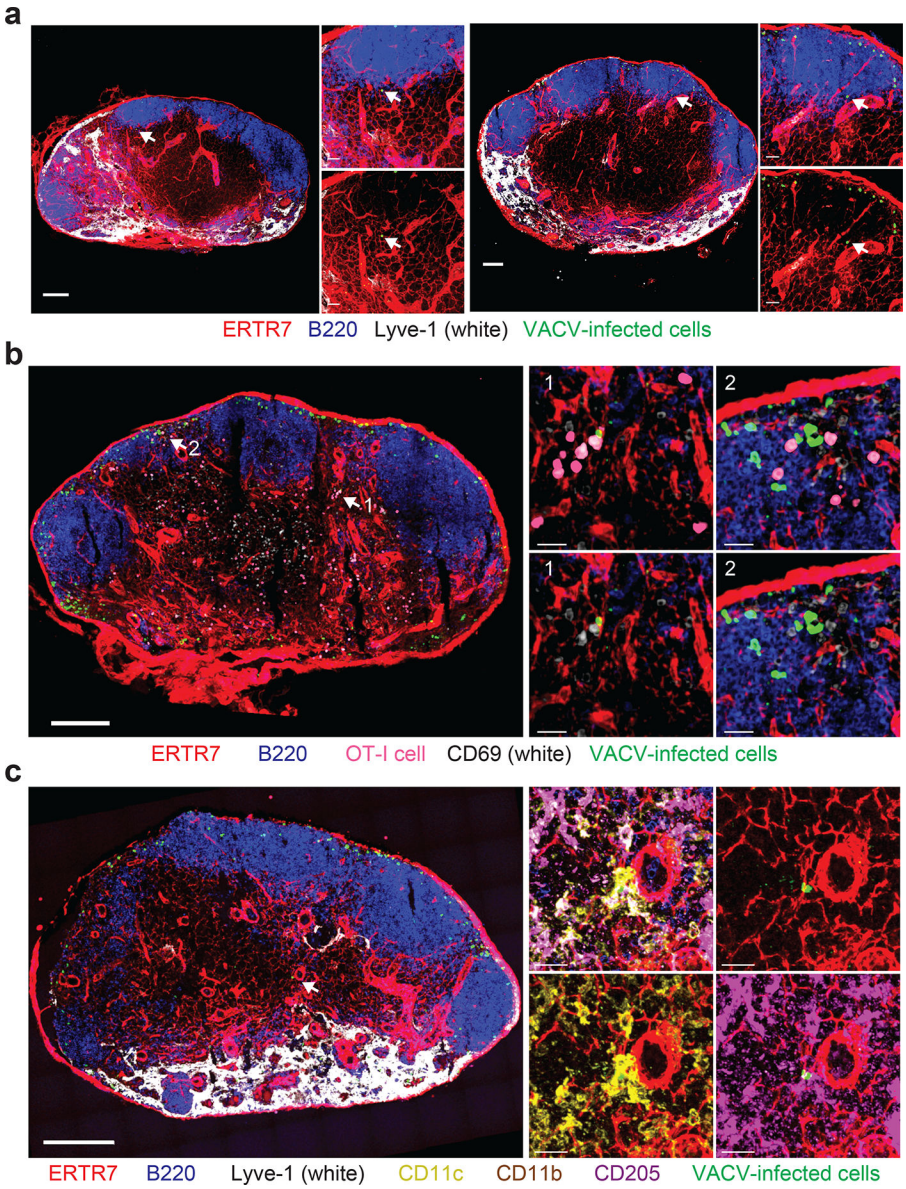

Figure 7. VACV infects paracortical DCs at lower viral doses.

a) Maximum intensity projection (MIPs) of sections from two different popliteal LNs (left and right) harvested 8 h after footpad injection of 10^6 pfu of VACV. ERTR7 = red, Lyve-1 = white, VACV-infected cells = green, B220 = blue. Arrows indicate the location of VACV-infected paracortical cell. scalebars = 100 μm. Higher magnification images are shown on the right; lower panels lack the blue channel for clarity. Scalebars = 50 μm. Results are representative of 10 LNs from 3 experiments. **b**) MIP of a section of a popliteal LN harvested 8 h after footpad injection of 10^6 pfu of VACV. Prior to infection, 10^6 OT-I $CD8^+$ T cells were transferred (pink). ERTR7 = red, B220 = blue, CD69 = white, VACV-infected cells = green. Arrows indicate two areas of T cell activation that are shown in higher magnification insets on the left. Scalebar = 200 μm. Top panels of insets show merge; bottom panels do not show OT-I signal (pink) in order to reveal CD69 staining more clearly. Scalebars = 20 μm. Results are representative of 10 LNs from 3 experiments. **c**) MIP of a

section of a popliteal LN harvested 8 h after footpad infection with 10^6 pfu of VACV showing an infected paracortical $CD205^+$ DC. Scalebar = 200 μm. Higher magnification images are shown in the insets showing: top left) merge; top right) conduits + VACV-infected cells; lower left) conduits + VACV-infected cells + CD11c + CD11b; lower right) conduits + VACV-infected cells + CD205. Scalebar = 20 μm. ERTR7 = red, Lyve-1 = white, VACV-infected cells = green, B220 = blue, CD11c = yellow, CD205 = purple, and CD11b = brown. Results are representative of 10 LNs from 3 experiments.

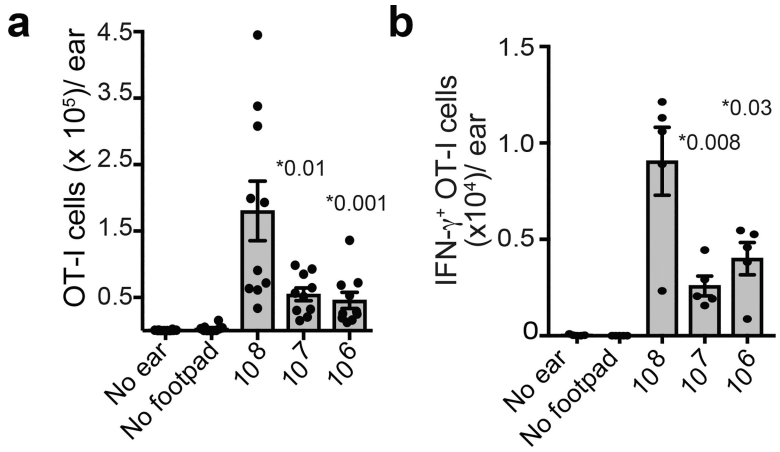

Figure 8. T cells activated at the highest viral doses traffic rapidly to the infected tissue.

a) Number of T cells in the ear at the indicated viral dose. (For no ear, only footpad infection was given. For no footpad, only ear infection was given). Dots show individual ears. n = 10 ears from 5 mice. **b**) Number of IFN-γ producing OT-I $CD8^+$ T cells in the ear after infection with indicated viral dose. Note that for these experiments, mice were infected in the ear pinna with VACV expressing SIINFEKL 24 h after footpad infection. Dots show individual animals. n = 5 ears from 5 mice. Statistics = unpaired two-tailed *t* test. For a and b, results were repeated 3 times with 5 mice/group.